Spatial and temporal variability of Antarctic ice sheet microwave brightness temperatures

David P. Schneider and Eric J. Steig

Department of Earth and Space Sciences, University of Washington, Seattle, WA USA

Received 16 November 2001; revised 16 May 2002; accepted 9 July 2002; published 22 October 2002.

[1] Annual and interannual variability of 21 years of passive microwave brightness temperatures on the Antarctic ice sheet is documented through principal component analysis. The leading modes show that brightness temperatures are dominantly forced by the annual temperature cycle, with surface melting signals explaining about 5% of the total variance of the data. Analysis of the data with the annual cycle and melting signals removed results in two significant interannual modes. The first is consistent with the Antarctic Oscillation and its influence on Antarctic surface temperatures, while the second reflects regional scale variability that appears to be linked to sea-ice anomalies and the El Niño-Southern Oscillation. The expression of these characteristic patterns of Southern Hemisphere climate variability on the Antarctic continent provides a framework for interpreting modern climate records, as well as a basis for reconstructing past climate variability with ice cores. *INDEX TERMS:* 9310 Information Related to Geographic Region: Antarctica; 3360 Meteorology and Atmospheric Dynamics: Remote sensing; 1863 Hydrology: Snow and ice (1827); 3309 Meteorology and Atmospheric Dynamics: Climatology (1620); 3349 Meteorology and Atmospheric Dynamics: Polar meteorology. **Citation:** Schneider, D. P., and E. J. Steig, Spatial and temporal variability of Antarctic ice sheet microwave brightness temperatures, *Geophys. Res. Lett.*, *29*(20), 1964, doi:10.1029/2002GL015490, 2002.

1. Introduction

[2] Recent studies of Antarctic surface temperatures have documented differences in trends among several stations around the continent. For instance, Antarctic Peninsula stations show a strong warming trend, while stations in other areas show no significant trend or slight cooling [*Comiso*, 2000]. These differences may in part be explained by climatic patterns such as the Antarctic Oscillation, the Antarctic Circumpolar Wave, and teleconnections to the El Niño-Southern Oscillation (ENSO) [*Thompson and Wallace*, 2000; *White and Peterson*, 1996; *Yuan and Martinson*, 2001] that have been identified in high southern latitudes. Over the Antarctic continent itself, however, the relative importance of these patterns is largely unknown due to the paucity of instrumental records.

[3] Passive microwave brightness temperature (T_b) data provide a tool for studying climate of the large polar ice sheets year-round in all weather conditions, and at relatively high spatial resolution [*Jezek et al.*, 1993; *Abdalati et al.*, 1995]. However, no study has used the full data set to document the dominant spatial and temporal characteristics of the data. In this study, we compile T_b data for the 37 GHz vertically-polarized (37 GHz v) channel into continuous series from 1979 to 1999, covering most of the Antarctic continent. We use principal component analysis (PCA) to determine the statistically most important patterns in the data. Their relationship to physical variables and climate is then assessed.

0094-8276/02/2002GL015490$05.00

2. Data and Methods

[4] The 37 GHz v data were collected by the Scanning Multichannel Microwave Radiometer (SMMR) instrument from November, 1978 until July, 1987 at every-other-day resolution, and the Special Sensor Microwave Imager (SSM/I) instruments (F8, F11, and F13) at daily resolution thereafter. We applied corrections to account for calibration differences in the instruments, combining the linear regression results of *Jezek et al.* [1993], *Abdalati et al.* [1995], and *Stroeve et al.* [1998]. All data were normalized to the SSM/I F8 baseline. Monthly means for the period January, 1979 to December, 1999 were derived from the 25 × 25 km gridded data provided by the National Snow and Ice Data Center (NSIDC).

[5] In microwave wavelengths, where the Rayleigh-Jeans approximation applies, T_b is a function of the physical temperature of the near-surface snow times its emissivity [*Zwally*, 1977]. Microwave emission at 37 GHz v is most strongly influenced by the top few tens of centimeters of the snowpack, comparable to the penetration depth of the diurnal temperature cycle [*Shuman et al.*, 1995]. Emissivity of snow is influenced by liquid water content, grain size, density, and crystal structure [*Zwally and Fiegles*, 1994]. Nonetheless, T_b is most strongly forced by the seasonal air temperature cycle, as shown by its high correlation with *in situ* and reanalysis records of surface temperature, as well as radiative transfer modeling studies [*Shuman et al.*, 1995; *Bingham and Drinkwater*, 2000].

[6] Microwave emissivity differences driven by the influence of snow accumulation rate may contribute significantly to spatial patterns in long term mean T_b, making separation of accumulation and air temperature effects on T_b difficult. However, these patterns are largely fixed in time [*Fily and Benoist*, 1991], and can be removed by using anomalies. On an interannual timescale, accumulation is poorly correlated with T_b, yet the high correlation of T_b with air temperature is significant as shown by *Bingham and Drinkwater* [2000]. Their study also points to an important caveat in interpreting T_b signatures: if an efficient scattering layer in the snow pack forms following melting or depth hoar development, T_b initially drops, followed by an upward trend that is especially pronounced if the accumulation rate is high. Below, we demonstrate that melting leads to a distinctive

signature in the variance structure of the data, and can be identified with PCA. Thus, on an interannual timescale, we can readily mask those areas where the influences of melting and accumulation are important. However, due to the possibility that subtler variations in snow properties influence T_b, we cannot conclude that interannual patterns in T_b constitute a pure surface temperature signal.

[7] In each set of PCA results discussed below, the two leading eigenvalues of the covariance matrix meet the separation criteria of *North et al.* [1982]. Their corresponding principal component (PC) and empirical orthogonal function (EOF) pairs are referred to as modes. PCs describe the amplitude and sign of the spatial EOF patterns through time. The EOF patterns are shown either as correlation coefficient maps, derived by regression of the PCs against the original T_b time series at each gridpoint, or as covariance maps, which display typical T_b amplitudes associated with one standard deviation of the respective PC.

3. Results

[8] We discuss two major sets of PCA results, showing seasonal and interannual characteristics of the T_b data. The leading mode of the monthly resolution 37 GHz v data accounts for 82% of the variance and represents the seasonal cycle. Spatially, seasonal amplitudes are greatest towards the high interior of the continent, which is consistent with station surface temperature data [*Comiso*, 2000]. The first PC (PC1) shows that the amplitude of the seasonal cycle has remained relatively constant, with some interannual variability apparent (Figure 1a). In agreement with the instrumental record of temperature [*King and Turner*, 1997], the seasonal cycle in PC1 is not symmetric: summer warmth is short lived in December and January, while winter remains cold for four to five months. The maintenance of the long or "coreless" winter [*van Loon*, 1967], often with a modest mid-winter warming as seen in PC1, has been related to the Southern Hemisphere semiannual oscillation (SAO). The SAO involves a twice-yearly wave in surface pressure with two contracting and two expanding phases of the circum-Antarctic low pressure belt [*Van den Broeke*, 2000]. In winter, the second expanded phase of the SAO allows for the meridional advection into Antarctica of relatively warm air from the extrapolar southern continents.

[9] The seasonal temperature cycle dominates the T_b field, yet the second mode explains 5% of the variance and deserves consideration. PC2 (Figure 1b) has an annual cycle with a much smaller amplitude and different phasing than PC1. High positive correlation values in Figure 1c imply that February is often the coldest month of the year in these regions. As this is not a reasonable temperature signal, T_b in these regions indicates reduced emissivity in late summer. This can be explained by periods of summer surface melting. As *Zwally and Fiegles* [1994] note, repeated melting and refreezing of snow grains near the surface leads to increased grain size, increasing the amount of radiative scattering and lowering T_b. When more melting occurs, the annual negative amplitude of PC2 is larger.

[10] Although a detailed reconstruction of individual melt events is not done in this study, we note that our results compare well with the melt index of *Zwally and Fiegles* [1994]. Both show that from 1979–1987, summer 1982/83 had the most extensive melt periods and 1985/86 had the least amount of melting. Furthermore, as indicated on Figure 1c, areas that are known to melt most often—the ice shelves around the Peninsula and the Amery ice shelf—have very high ($r \geq .7$) correlation coefficients with PC2, while areas that occasionally experience melting—the Ross Ice Shelf and Siple coast—have lower coefficients [*Zwally and Fiegles*, 1994; *Scambos et al.*, 2000]. In our analysis, 1991/1992 stands out as having the largest melt event in the entire 21-year time series.

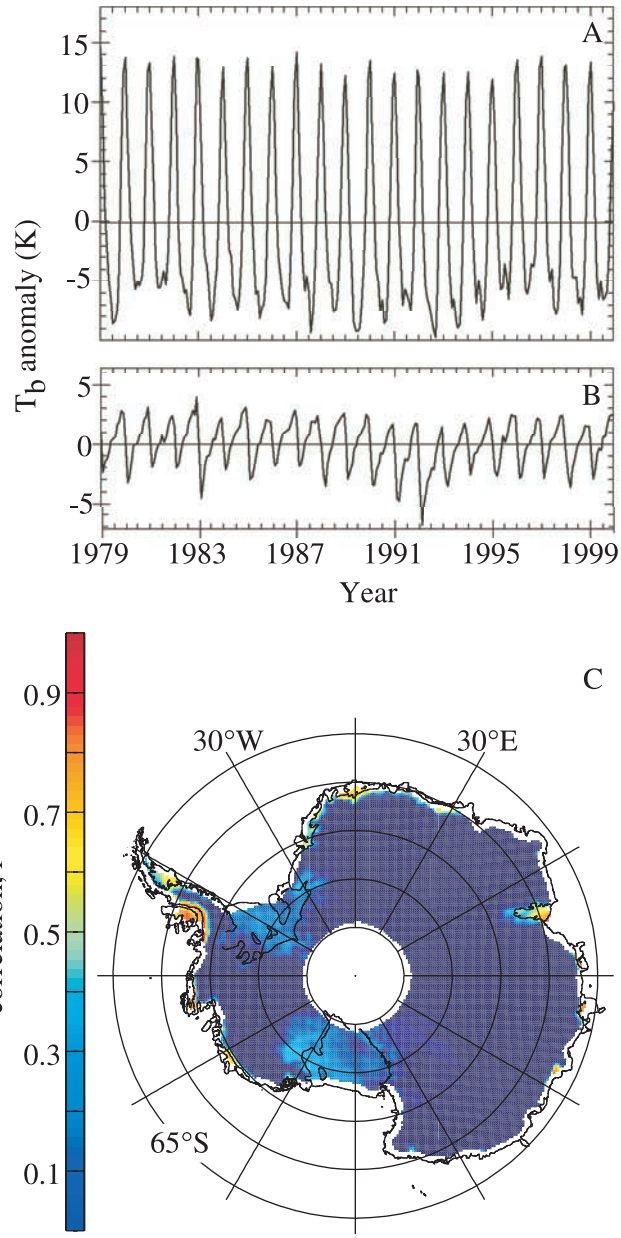

Figure 1. Results from PCA of monthly Antarctic 37 Ghz v T_b data. (a) PC1, the seasonal cycle. (b) PC2, a melting signal. Note the large negative amplitudes in 1982/83 and 1991/92 showing the largest melt events in the record. (c) Correlation map of PC2 with the original T_b data. Areas with $r \geq 0.3$ form the basis for the melt mask used in subsequent analyses. Pixels adjacent to the coast have been entirely excluded from this analysis.

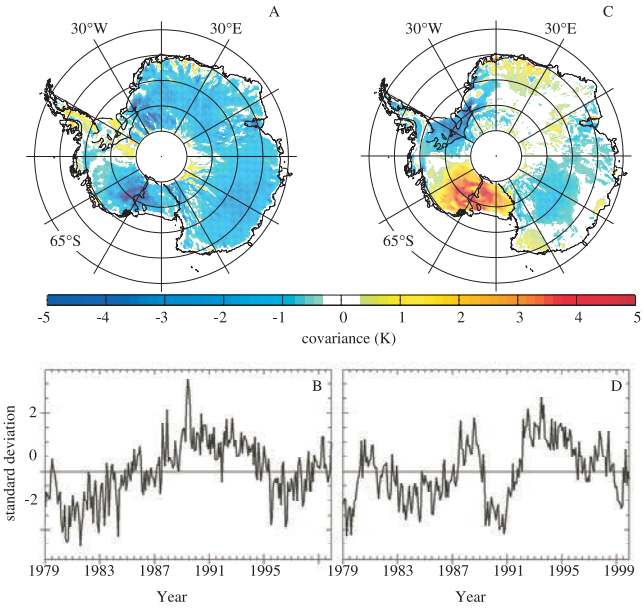

Figure 2. Results from PCA of monthly anomalies of 37 GHz v T_b data. (a) The leading interannual EOF shown as a covariance map. (b) The leading PC. (c) As in (a) for the second interannual EOF. (d) PC of second interannual mode.

[11] To reduce the contribution of longer-term melting effects on our interannual analysis, we eliminate those pixels where the correlation map (Figure 1c) shows a correlation of $r \geq 0.3$. Additionally, we subtract the variance of the second mode from the remaining data so that only structures orthogonal to the melting mode are left. Combining these two steps forms a melt mask that largely eliminates melting effects, which is then used to create a data set for interannual PCA analyses. Although inspection of individual time series found the $r = 0.3$ threshold to be adequate, an additional test used an $r = 0.2$ cutoff. This lower threshold clearly eliminates all pixels that melted in the large 1991/92 event, as an examination of T_b signatures from that year reveals (not shown). Using threshold values less than 0.3 has no significant effect on the results discussed below; we use $r = 0.3$ for illustration because it retains a larger area of the ice sheet surface.

[12] After accounting for the influence of melting as discussed above, T_b anomalies were obtained by subtracting the monthly 1979–1999 climatology from the data. Masked areas, while not included in the PCA calculations themselves, are retained for illustration in the calculation of covariance maps. Two leading modes are resolved, accounting for 25% and 18% of the total variance respectively. In the leading EOF (Figure 2a), the overall pattern is negative covariance for most of the continent, with larger positive covariance primarily on the Antarctic Peninsula. The first PC (Figure 2b) shows low frequency variability on top of the interannual variability.

[13] The second EOF (Figure 2c) shows an anti-phase pattern between the Ronne-Filchner Ice Shelf and the Marie Byrd Land and Ross Ice Shelf regions. Spectral analysis by the multitaper method [*Mann and Lees*, 1996] reveals a broad peak in the second PC (Figure 2d) with a period between 3.8 and 5.2 years at the 99% confidence level.

[14] To further assess the significance of the leading modes identified, we repeated several identical PCAs on independent subsets of the data, including summer (October–March), winter (April–September), SMMR data alone, and SSM/I data alone. Both of the two leading modes found in the full time series exist in the summer only, winter only, and SSM/I series, while only the first mode is resolved in the shorter SMMR data set. The pattern associated with the second mode explains relatively more variance in the winter months. Given that the first mode is resolved in all four subsets of the T_b anomalies and that the second mode is resolved in all but the SMMR series, it is unlikely that the observed patterns are related to instrumental biases, such as calibration differences with the different microwave sensors. This test also supports the idea that the resolved modes reflect a stronger influence of temperature rather than emissivity variations. Because snow surface properties (notably grain size) and emissivity display strong seasonal variations [*Shuman et al.*, 1995; *Gow*, 1969], any significant influence not already excluded by the melt mask should be seen in a contrast between winter and summer EOF patterns.

4. Discussion

[15] The PCA results corroborate several features of Antarctic climatology that have been noted from the ground-based instrumental temperature records [*King and Turner*, 1997], while providing an improved spatial picture of those features. Important aspects of seasonal variability in T_b include: (1) greater seasonal contrast in the interior of Antarctica than the coast; (2) prevalence of the coreless winter throughout the continent; (3) modulation of temperatures by the semiannual oscillation; and (4) summer melt events on the ice shelves. That these features are dominant in T_b data suggests that T_b changes are primarily driven by temperature forcing. The largest non-temperature forcing, the melting signal, can be identified with our approach and removed from the data. However, variations in snow surface properties related to accumulation cannot be ignored and their influence on T_b warrants further research. Below, we show that significant correspondence exists between the dominant interannual modes of T_b and those previously identified in other Southern Hemisphere climate variables.

[16] The leading interannual mode of T_b bears a strong resemblance to the pattern of temperature anomalies associated with the Southern Hemisphere annular mode (AAO). *Thompson and Wallace* [2000] define the AAO as the first EOF of the NCEP-NCAR reanalysis 850 hPa geopotential height field anomalies poleward of 20° S. The AAO captures the dominant interannual variability in extratropical atmospheric circulation and involves an oscillation of atmospheric mass between the middle and high southern latitudes, explaining 50% or more of the variance in sea level pressure above Antarctica. In the regression of the corresponding PC (AAO index) on surface temperature anomalies from Antarctic research stations, the Antarctic Peninsula region is out of phase with the rest of the continent [*Thompson and Wallace*, 2000]. Regression of the AAO index upon the T_b anomalies results in a comparable pattern (Figure 3), which in turn is similar to the leading EOF of T_b (Figure 2a). The monthly AAO index and PC1 of T_b are significantly correlated at $r = 0.42$. This

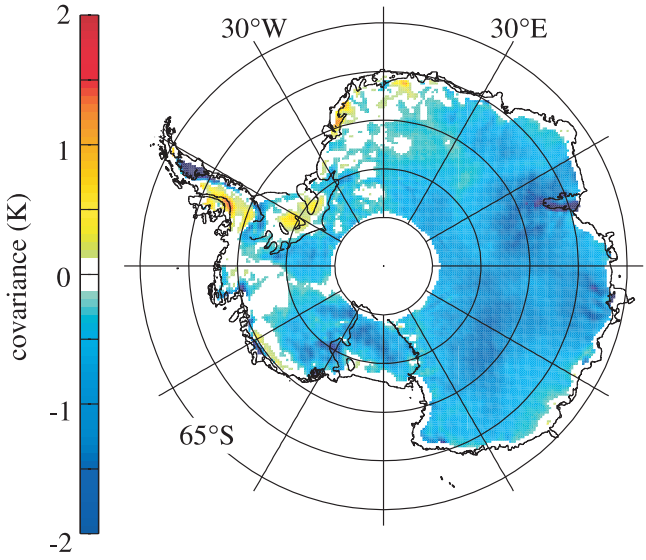

Figure 3. Regression of the Antarctic Oscillation index [*Thompson and Wallace*, 2000] against T_b anomalies.

suggests that a large part of the variance in our leading interannual mode may be explained by AAO dynamics.

[17] In contrast to the large scale of the AAO, our second interannual mode appears to reflect regional scale climatic influences. Analyses of sea-ice extent show maximum variances in the Amundsen, Ross, and Weddell Sea regions, adjacent to the Ross and Ronne-Filchner ice shelves, where our maximum variances also appear. *Yuan and Martinson* [2001] link this pattern to the propagating Antarctic Circumpolar Wave (ACW) previously identified by *White and Peterson* [1996], although they emphasize that the dominant variance in the ACW pattern is actually a stationary wave they name the "Antarctic Dipole." In their analysis, the corresponding PC has a spectral peak at a period of 5 years, within the 3.8 to 5.2 year range for PC2 of T_b anomalies These time scales are associated with ENSO, and there likely is an intimate relationship among the Antarctic Dipole, ACW, and ENSO that has yet to be fully understood.

5. Conclusions

[18] Surface temperatures in Antarctica should reflect the same ocean and atmospheric dynamics that influence sea-ice extent and the large-scale patterns of sea surface temperature, atmospheric pressure, and winds. Our results demonstrate that signatures of these dynamics—the AAO and ENSO-related patterns—are expressed in Antarctic T_b data. The spatial picture of climate variability available from satellites thus provides a useful basis for interpretation of instrumental station data as well as paleoclimate proxy data from ice cores. With respect to the latter, it is notable that the expression of the ENSO-related signal in the interannual EOF of T_b has maximum variance in the area of the Siple Coast. This suggests that this area would be optimal for using ice core data to extend records of ENSO-related variability beyond the available instrumental record. Preliminary analyses of stable isotopes—which indirectly reflect air temperature—from ice cores at Siple Dome do indeed show significant variance in the ENSO band [*White et al.*, 1999]. Future work will include the utilization of independent data, including infrared-based AVHRR satellite surface temperature retrievals [*Comiso*, 2000], enabling an improved assessment of microwave emissivity variations. These data, combined with the longer time scale of new high-resolution ice core records, will help to better characterize Antarctic climate variability.

[19] **Acknowledgments.** This work was supported by the U.S. National Science foundation (OPP-0196105) in association with the U.S. ITASE program. The authors also thank the NSIDC in Boulder, CO for providing the SMMR and SSM/I data on CD-ROM. We thank two anonymous reviewers for their constructive comments.

References

Abdalati, W., K. Steffen, C. Otto, and K. C. Jezek, Comparison of brightness temperatures from SSMI instruments on the DMSP F8 and F11 satellites for Antarctica and the Greenland ice sheet, *Int. J. Remote Sens.*, *16*(7), 1223–1229, 1995.

Bingham, A. W., and M. Drinkwater, Recent changes in the microwave scattering properties of the Antarctic ice sheet, *IEEE Trans. Geosci. Rem. Sens.*, *38*(4), 1810–1820, 2000.

Comiso, J. C., Variability and trends in Antarctic surface temperatures from in situ and satellite infrared measurements, *J. Climate*, *13*, 1674–1696, 2000.

Fily, M., and J. Benoist, Large-scale statistical study of Scanning Multichannel Microwave Radiometer (SMMR) data over Antarctica, *J. Glaciol.*, *37*(125), 129–137, 1991.

Gow, A. J., On the rates of growth of grains and crystals in south polar firn, *J. Glaciol.*, *8*(53), 241–252, 1969.

Jezek, K. C., C. J. Merry, and D. J. Cavalieri, Comparison of SMMR and SSM/I passive microwave data collected over Antarctica, *Ann. Glaciol.*, *17*, 131–136, 1993.

King, J. C., and J. Turner, *Antarctic Meteorology and Climatology*, Cambridge University Press, Cambridge, 1997.

Mann, M. E., and J. M. Lees, Robust estimation of background noise and signal detection in climatic time series, *Clim. Change*, *33*, 409–445, 1996.

North, G. R., T. L. Bell, and R. F. Cahalan, Sampling errors in the estimation of empirical orthogonal functions, *Mon. Weather Rev.*, *110*, 699–706, 1982.

Scambos, T. A., C. Hulbe, M. Fahnestock, and J. Bohlander, The link between climate warming and break-up of ice shelves in the Antarctic Peninsula, *J. Glaciol.*, *46*(154), 516–530, 2000.

Shuman, C. A., R. B. Alley, S. Anandakrishnan, and C. R. Stearns, An empirical technique for estimating near-surface air temperature trends in central Greenland from SSM/I brightness temperatures, *Remote Sens. Environ.*, *51*, 245–252, 1995.

Stroeve, J., J. Maslanik, and L. Xiaoming, An intercomparison of DMSP F11- and F13-derived sea ice products, *Remote Sens. Environ.*, *64*, 132–152, 1998.

Thompson, D. W. J., and J. M. Wallace, Annular Modes in the extratropical circulation. Part I: Month-to-month variability, *J. Climate*, *13*, 1000–1016, 2000.

Van den Broeke, M., The semiannual oscillation and Antarctic climate, part 5: Impact on the annual temperature cycle as derived from the NCEP/NCAR reanalysis, *Climate Dyn.*, *16*, 369–377, 2000.

van Loon, H., The half-yearly oscillations in middle and high southern latitudes and the coreless winter, *J. Atmos. Sci.*, *24*, 472–486, 1967.

White, J. W. C., E. J. Steig, J. Cole, E. R. Cook, and S. J. Johnsen, Recent, annually resolved climate as recorded in stable isotope ratios in ice cores from Greenland and Antarctica, *Amer. Met. Soc. Sym. Glob. Clim. Change Stud.*, *10*, 300–302, 1999.

White, W. B., and P. G. Peterson, An Antarctic circumpolar wave in surface pressure, wind, temperature and sea-ice extent, *Nature*, *380*, 699–702, 1996.

Yuan, X., and D. G. Martinson, The Antarctic dipole and its predictability, *Geophys. Res. Lett.*, *28*(18), 3609–3612, 2001.

Zwally, H. J., Microwave emissivity and accumulation rate of polar firn, *J. Glaciol.*, *18*(79), 195–215, 1977.

Zwally, H. J., and S. Fiegles, Extent and duration of Antarctic surface melting, *J. Glaciol.*, *40*(136), 463–476, 1994.

D. P. Schneider and E. J. Steig, Department of Earth and Space Sciences, University of Washington, Box 351310, Seattle, WA 98195, USA. (schneidd@u.washington.edu)